

Abstract of thesis entitled

# This is the title of my thesis

Submitted by

**Cheuk Yee LO**

for the degree of Doctor of Philosophy  
at The University of Hong Kong  
in August 2018

These are the motivations. These are the methods. These are the results.  
These are the discussions. These are the significance.

---

*An abstract of exactly 499 words*

# **This is the title of my thesis**

by

**Cheuk Yee LO**

A thesis submitted in partial fulfilment of the requirements for  
the Degree of Doctor of Philosophy  
at The University of Hong Kong.

August 2018

# **Declarations**

I declare that this thesis represents my own work, except where acknowledgement is made, and that it has not been previously included in a thesis, dissertation or report submitted to this University or to any other institution for a degree, diploma or other qualifications.

Signed .....  
.....

Cheuk Yee LO

# Acknowledgments

This command generate dummy text. Remove this line and replace it by your words of appreciation.

# Contents

<b>Abstract</b>	i
<b>Title Page</b>	ii
<b>Declaration</b>	iii
<b>Acknowledgments</b>	iv
<b>Contents</b>	v
<b>List of Figures</b>	vii
<b>List of Tables</b>	ix
<b>List of Abbreviations and Symbols</b>	x
<b>1 Theoretical Background</b>	1
1.1 Introduction . . . . .	1
1.2 Standard Model . . . . .	1
1.2.1 Matter particles . . . . .	2
1.2.2 Forces and carrier particles . . . . .	3
1.2.3 Feynman diagram . . . . .	3
1.3 Limitation of Standard Model . . . . .	3
1.3.1 Dark matter . . . . .	3
1.3.2 Hierarchy problem . . . . .	5
1.3.3 Unification of forces . . . . .	6
1.4 Supersymmetry . . . . .	6
1.4.1 Minimal Supersymmetric Standard Model . . . . .	7
1.5 Wh channel . . . . .	7

<b>2 Experimental Setup</b>	<b>8</b>
2.1 Introduction . . . . .	8
2.2 The Large Hadron Collider . . . . .	8
2.3 ATLAS detector . . . . .	10
2.3.1 coordinate system . . . . .	12
2.3.2 magnetic system . . . . .	12
2.3.3 The inner detector . . . . .	12
2.3.4 Calorimeter . . . . .	17
2.3.5 Muon Spectrometer . . . . .	17
<b>3 Pre-selection</b>	<b>18</b>
3.1 Trigger selection . . . . .	18
3.2 Event selection . . . . .	18
3.3 Object definitions . . . . .	18
3.3.1 electrons and muons . . . . .	18
3.3.2 jets . . . . .	18
3.3.3 Missing transverse energy . . . . .	18
<b>4 Signal Region</b>	<b>19</b>
<b>5 Background estimation</b>	<b>20</b>
5.1 charge flip background . . . . .	20
5.1.1 Sources for charge flip background . . . . .	20
5.1.2 Likelihood method . . . . .	22
5.1.3 Background subtraction . . . . .	24
5.1.4 Results without systematic uncertainty . . . . .	24
5.1.5 Systematic uncertainties due to background subtraction . . . . .	26
5.1.6 Systematic uncertainties due to likelihood method . . . . .	26
5.1.7 Results with total uncertainties . . . . .	28
5.1.8 MC validation . . . . .	29
5.2 fake lepton background . . . . .	31
<b>6 Validation regions</b>	<b>32</b>
<b>References</b>	<b>33</b>

# List of Figures

1.1	The table for all fundamental particles in SM. [1]	2
1.2	All allowed fundamental Feynman vertices in SM, except higgs-related vertices. [2]	4
1.3	All allowed fundamental higgs-related Feynman vertices in SM.	5
2.1	The schematic diagram of the CERN accelerator complex, which shows a series of accelerators and facilities. [3]	9
2.2	The cut-away view of the ATLAS detector. It is 25m high and 44m long. [4]	11
2.3	The cross section of the ATLAS detector. This shows different components of the ALTAS and how ATLAS detect different types of particles [5]	11
2.4	The whole structure of the ATLAS inner detector. [6]	13
2.5	The distances R from the beam for the 3 components: pixel, SCT and TRT. [6]	14
2.6	The shapes, the orientations and the $\eta$ coverage for each sensor. [7]	15
2.7	whole calorimeter [8]	16
2.8	muon spectrometer [9]	17
5.1	This shows how the track of the electron is incorrectly reconstructed (the orange track), due to the process of bremsstrahlung and $\gamma$ conversion.	21
5.2	This shows how the track of the electron is incorrectly reconstructed (the orange track), due to very high $p_T$ of the electron.	21
5.3	The measured values of the charge-flip rate $\epsilon_i$ in data. Only uncertainties due to the likelihood method are included.	25

5.4	The systematic variations of the charge-flip rate $\epsilon_i$ in data, due to the background subtraction. . . . .	27
5.5	This diagram shows how the original electron is found through the decay chain. . . . .	27
5.6	The comparison between the likelihood method and the MC truth method, by using the $Z \rightarrow ee$ MC samples. Hence, the systematic uncertainties due to likelihood method can be estimated. . . . .	29
5.7	The measured values of the charge-flip rate $\epsilon_i$ in data, with total uncertainties. . . . .	30
5.8	The comparison between the weighted OS events and the SS events, with different variables. . . . .	31

# List of Tables

5.1 Binning in $p_T$ and $ \eta $ for the charge-flip rate $\epsilon_i$ .	22
---	----

# List of Abbreviations and Symbols

LHC Large Hadron Collider

SUSY Supersymmetry

# Chapter 1

## Theoretical Background

### 1.1 Introduction

Particle physics is a branch of physics that studies the most fundamental particles and their interaction. We believe that all matter and radiation in the universe are made up of these fundamental particles, and their behaviour is described by the theories in particle physics. In 20th century, our understanding about the nature of fundamental particles has had great breakthrough and advance. Also, many particle colliders have been built to give much insight to develop the theories and test the theories. The currently mainstream theory of particle physics is called the Standard Model.

### 1.2 Standard Model

Standard Model(SM) is the current theory to describe the fundamental particles in particle physics. It has already gained huge success in predicting the experimental results, including the prediction of existence of the top quark, the tau neutrino, and the Higgs boson. It has also explained almost all experimental results with high accuracy. It represents our best understanding of how the fundamental particles interact with each other.

Physicists discovered that there are 4 fundamental force in the universe: electromagnetic force, weak force, strong force, and gravitational force. However, SM can only describe 3 of them: electromagnetic, weak and strong interaction, and the gravity cannot be described by SM. Figure 1.1 shows all fundamental particles in SM, and their mass, electric charge and spin. All matter is made up of

# Standard Model of Elementary Particles

three generations of matter (fermions)					
	I	II	III		
mass	$\approx 2.4 \text{ MeV}/c^2$	$\approx 1.275 \text{ GeV}/c^2$	$\approx 172.44 \text{ GeV}/c^2$	0	$\approx 125.09 \text{ GeV}/c^2$
charge	2/3	2/3	2/3	0	0
spin	1/2	1/2	1/2	1	0
	u	c	t	g	H
	up	charm	top	gluon	Higgs
QUARKS	$\approx 4.8 \text{ MeV}/c^2$	$\approx 95 \text{ MeV}/c^2$	$\approx 4.18 \text{ GeV}/c^2$	0	$\approx 125.09 \text{ GeV}/c^2$
	-1/3	-1/3	-1/3	0	0
	1/2	1/2	1/2	1	0
	d	s	b	$\gamma$	photon
	down	strange	bottom		
	$\approx 0.511 \text{ MeV}/c^2$	$\approx 105.67 \text{ MeV}/c^2$	$\approx 1.7768 \text{ GeV}/c^2$	0	$\approx 91.19 \text{ GeV}/c^2$
	-1	-1	-1	1	1
	1/2	1/2	1/2	Z	Z boson
	e	$\mu$	$\tau$		
LEPTONS	$<2.2 \text{ eV}/c^2$	$<1.7 \text{ MeV}/c^2$	$<15.5 \text{ MeV}/c^2$	0	$\approx 80.39 \text{ GeV}/c^2$
	0	0	0	1	1
	1/2	1/2	1/2	$W$	W boson
	$\nu_e$	$\nu_\mu$	$\nu_\tau$		
	electron neutrino	muon neutrino	tau neutrino		
SCALAR BOSONS					
GAUGE BOSONS					

Figure 1.1: The table for all fundamental particles in SM. [1]

fermions (purple and green), which is the first 3 columns in figure 1.1. Fermions are divided into two groups: quarks(purple) and leptons(green). The forces between the fermions are mediated by the force carriers, which is gauge bosons(red). Higgs bosons(yellow) is scalar bosons, which give mass to other massive particles.

## 1.2.1 Matter particles

There are 6 types of quarks: up quarks(u), down quarks(d), charm quarks(c), strange quarks(s), top quarks(t) and bottom quarks(b). Quarks interacts with strong interaction, while leptons does not. There are 3 types of charged leptons: electrons, muons and taus. There are 3 types of neutral leptons: electron neutrinos, muon neutrinos and tau neutrinos. The first column is the first generation, which is the lightest and most stable particles. Hence, normal matter in our daily life is made from the particles in the first generation. The second and third col-

umn are the second and third generation respectively, which is heavier and less stable particles. These particles will finally decay into the particles in the first generation. Due to the phenomenon of neutrino oscillation, neutrinos should have non-zero masses, but their value are still uncertain in our current technology.

### 1.2.2 Forces and carrier particles

Photon is the force carrier for electromagnetic interaction. Gluon is the force carrier for strong interaction. Z and W boson is the force carrier for weak interaction. The effects of these fundamental forces stem from the exchange of the corresponding force carrier. These forces also have different strengths and different ranges. Strong force is the strongest force, while the electromagnetic force is in the middle. The weak force is the weakest force among the three, but it still much much stronger than the gravity. The electromagnetic force has infinite range, while the strong and weak forces have very short ranges at the level of subatomic particles.

For example, a proton is composed of two up quarks and one down quark, and a neutron is composed of one up quark and two down quarks. The forces between quarks inside the proton are mediated by gluons.

### 1.2.3 Feynman diagram

The fundamental interactions among these fundamental particles are described by the allowed fundamental Feynman vertices. All allowed fundamental Feynman vertices in SM are shown in figure 1.2 and 1.3. These fundamental vertices are the basic building blocks for all physical processes, by jointing these vertices together.

## 1.3 Limitation of Standard Model

Although Standard Model can explain almost all experimental results, there still are some phenomena it cannot explain.

### 1.3.1 Dark matter

Dark matter is some unknown matter that does not involve in electromagnetic interaction, but involve in gravitational interaction. It was first discovered in the Milky Way, by studying the speed of the stars orbiting around the center of the Milky Way. Because it does not involve in electromagnetic interaction, it does

## Standard Model Interactions (Forces Mediated by Gauge Bosons)

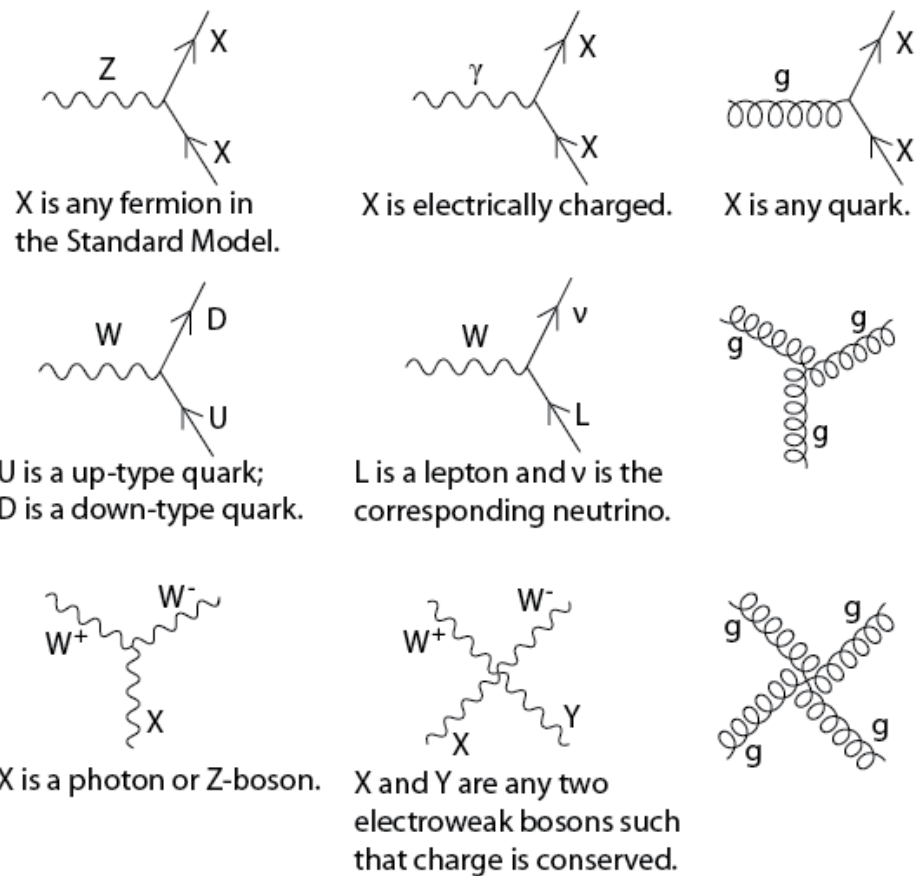


Figure 1.2: All allowed fundamental Feynman vertices in SM, except higgs-related vertices. [2]

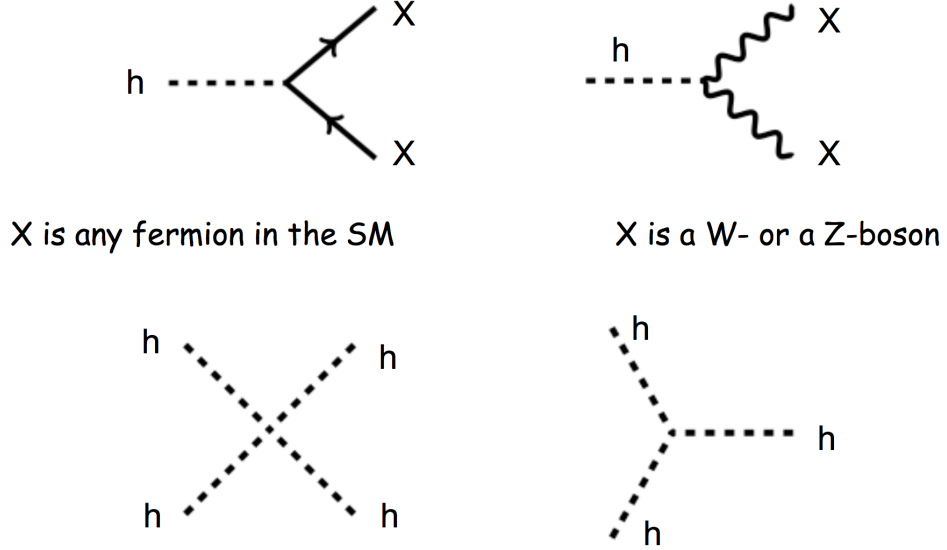


Figure 1.3: All allowed fundamental Higgs-related Feynman vertices in SM.

not emit any electromagnetic radiation, and it cannot be seen by our telescopes. However, SM cannot explain the nature of dark matter, and what dark matter is made of.

### 1.3.2 Hierarchy problem

The hierarchy problem is the question why the weak force is stronger than the gravitational force by  $10^{24}$  times. It is also asked why the mass of Higgs boson ( $\sim 125$  GeV) is much lighter than the Planck mass ( $\sim 10^{19}$  GeV).

The Lagrangian for the interaction term between the fermion Dirac field  $\psi$  and the Higgs field  $h$  (i.e. Yukawa interaction) is given by

$$\mathcal{L}_{\text{Yukawa}} = -\lambda \bar{\psi} h \psi \quad (1.1)$$

where  $\lambda$  is the Yukawa coupling constant. The quantum correction to the square of the Higgs mass  $\Delta m_H^2$  is then given by

$$\Delta m_H^2 = -\frac{|\lambda|^2}{16\pi^2} \Lambda^2 + \dots \quad (1.2)$$

where  $\Lambda$  is the energy scale up to which the Standard Model is valid, namely the Planck scale ( $\sim 10^{19}$  GeV). Because  $\Lambda$  is quadratic divergent, the correction to the Higgs mass is in the order of Planck scale. Unless there are very delicate cancellation between the correction terms, the Higgs mass should be in the order

of Planck scale. But, we found that the experimental Higgs mass is in the order of 125 GeV, and this is called the hierarchy problem.

### 1.3.3 Unification of forces

In the 1860s, James Clerk Maxwell wrote down his famous equations Maxwell's equations, which unified two different phenomena: electricity and magnetism. Due to this unification, we now understand that electricity and magnetism are two different manifestations of the same phenomenon, and we now call it electromagnetism.

Similar thing happened in 1970s, physicists developed a theory that unified two fundamental forces: electromagnetic force and weak force. At the energy scale above 246 GeV, these two forces will merge into a single force: electroweak force. This unification predicted the existence of weak neutral current and a force carrier to carry this weak force. This force carrier was later confirmed experimentally in CERN, and it is now called the Z boson.

After that, an effect of strong force was found experimentally that the strong force becomes weaker when the energy is higher. This may indicate that electroweak force and strong force will become a single force at even high energy. However, the energy scale at which these forces are the same is much larger than the energy the particle accelerators can reach. There are some theories beyond the Standard Model that try to unify these force, such as supersymmetry.

## 1.4 Supersymmetry

Supersymmetry(SUSY) is an extension of the Standard Model, and try to answer some questions which the Standard Model cannot explain mentioned in section 1.3. One of the problem SUSY can solve is the hierarchy problem of Higgs mass mentioned in section 1.3.2. We first notice that the negative sign in the equation 1.2 is due to the correction from the fermions. If we can somehow have some symmetry between the fermions and bosons, and add more positive correction terms due to the bosons, the correction terms will cancel with each other and the hierarchy problem can be solved. This new symmetry is called the supersymmetry(SUSY).

#### **1.4.1 Minimal Supersymmetric Standard Model**

Minimal Supersymmetric Standard Model(MSSM) is the minimal supersymmetrical theory that contain the least number of new particle states and new interactions. It predicts that each particle in the Standard Model has its own partner particle, called the superpartner. The name of the superpartner is by adding a prefix "s", followed by the name of the orginal Standard Model particle. For example, the superpartner of an electron is called selectron. As for the symbol for the superpartner, a tilde will be added above the original symbol. For example, the symbol for selectron is  $\tilde{e}$ . Also, the spin of the superpartner will differ from the Standard Model particle by 1/2. For fermions, the spin of their superpartner is 0, while for bosons, the spin of their superpartner is 1/2. This is the new symmetry between the fermions and bosons, mentioned before. It is also the correction terms from these superpartners to fix the hierarchy problem of the Higgs mass. If MSSM is correct, these supersymmetric particles should be detected in the LHC.

### **1.5 Wh channel**

# Chapter 2

## Experimental Setup

### 2.1 Introduction

Our experimental data was collected from the ATLAS particle detector in the Large Hadron Collider (LHC). The following section will introduce LHC and the ATLAS particle detector.

### 2.2 The Large Hadron Collider

The Large Hadron Collider (LHC) was built in the border between France and Switzerland by the European Organization for Nuclear Research (CERN). It is a circular particle collider under the ground with circumference 27 km. Two beams of protons will be accelerated in opposite directions, to almost the speed of light, and then these two beams will collide with each other at the collision point. The energy of each beam is 6.5 TeV, and hence the center-of-mass energy of the two beams  $\sqrt{s}$  is 13 TeV, which is the energy used in this experiment. This energy is equivalent to the speed that the beam will circulate the ring 11,245 times per second. Under this high energy, new physics phenomena will happen, including SUSY. Figure 2.1 shows the schematic diagram of the CERN accelerator complex, which contains a series of accelerators, from low energy to high energy. The dark blue big circle in figure 2.1 represents the LHC, on which there are 4 particle detectors at 4 different interaction points (yellow points): ATLAS, CMS, LHCb and ALICE. By analyzing these collisions, we can have a deeper understanding of the laws of nature.

Before the beam is injected into LHC, the protons need to be accelerated by a

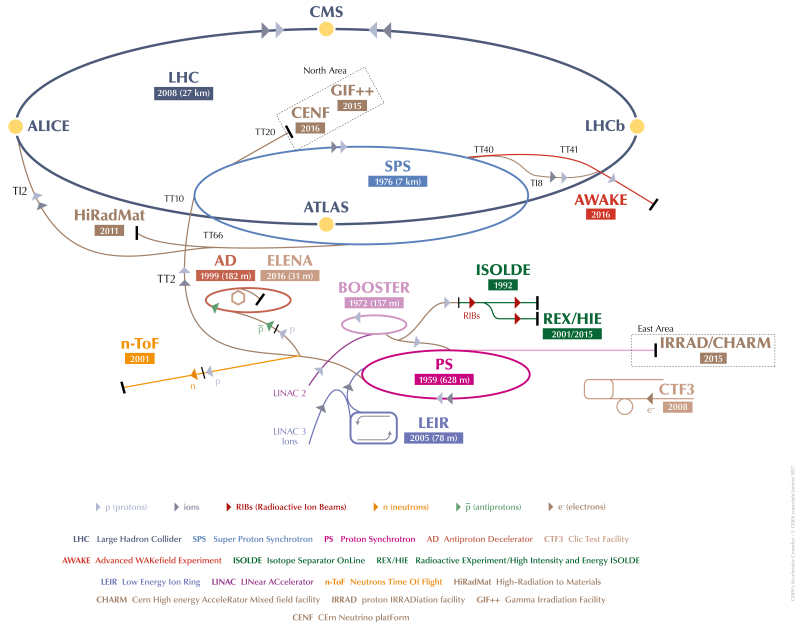


Figure 2.1: The schematic diagram of the CERN accelerator complex, which shows a series of accelerators and facilities. [3]

series of accelerators. The journey of the protons starts from a tank of hydrogen gas. The proton and the electron are separated by a electric field. The protons are then accelerated to 50 MeV by Linac2, which is a linear accelerator. The beam is then injected to the second accelerator called the Proton Synchrotron Booster (PSB), which accelerates the beam to 1.4 GeV. The beam is then injected to the third accelerator called the Proton Synchrotron (PS), which pushes the beam to 25 GeV. The beam is then injected to the fourth accelerator called the Super Proton Synchrotron (SPS), which further pushes the beam to 450 GeV. Finally, the beam is injected to the two beam pipes of the LHC. One of the beam moves in clockwise direction, while another beam moves in anti-clockwise direction. Two beams will be collided at the collision point inside the ATLAS detector. [10]

The circular path of the proton beam is maintained by many superconducting electromagnets along the LHC tunnel. There are 1232 main magnetic dipoles, and each of them generates a large magnetic field of 8.3 T. In order to generate such a high magnetic field, the coils need to have very high current of 11,080 A, and hence superconducting coil need to be used, to reduce the heat loss due to the electrical resistance. The material of superconducting coil is niobium-titanium

(NbTi). To reach the condition for superconductivity, the electromagnets operate at a very low temperature of 1.9 K. There are also 392 magnetic quadrupole to squeeze the proton beam, so that the chance of proton-proton collision will be higher. [11, 12]

The protons in the beam are grouped into different bunches, and there are about  $10^{11}$  protons in each bunch. The time-spacing between two adjacent bunches is 25ns (or 50 ns in the old configuration). This means that in each 25 ns, two bunches are collided at the collision point. For each bunch collision, there are about 10 to 50 proton-proton interaction. Hence, about  $10^9$  proton-proton collisions are produced in one second.

The interacting rate for a physics process  $\frac{dN}{dt}$  is the product of the cross section of that physics process  $\sigma$  and the instantaneous luminosity  $\mathcal{L}$ .

$$\frac{dN}{dt} = \sigma \mathcal{L} \quad (2.1)$$

The instantaneous luminosity  $\mathcal{L}$  is a measure of the interacting rate of two protons at the collision point, which is related to the density of the protons and the speed of the protons. The instantaneous luminosity in this experiment is about  $10^{34}$   $\text{cm}^{-2} \text{s}^{-1}$  (or  $10 \text{ nb}^{-1} \text{s}^{-1}$ ).

## 2.3 ATLAS detector

A Toroidal LHC ApparatuS (ATLAS) is the particle detector used in this experiment [7]. Figure 2.2 shows the main components of the ATLAS detector. The ATLAS detector is a general purpose particle detector, which is consisted of 3 main components: the inner detector, the calorimeter and the muon spectrometer. Figure 2.3 shows how the ATLAS distinguishes different types of particle. The inner detector can detect the paths of the charged particles. Photons and electrons will deposit most of their energy in the electromagnetic calorimeter, and finally stop by it. Hadrons(including protons and neutrons) and mesons will similarly stop by the hadronic calorimeter. Only muons and the neutrinos can reach the outermost muon spectrometer, but only muons can be detected by the muon spectrometer. Nearly all neutrinos will escape the whole ATLAS detector, which leads to some missing energy. In this design, different particles can be identified due to their signature in different parts of ATLAS.

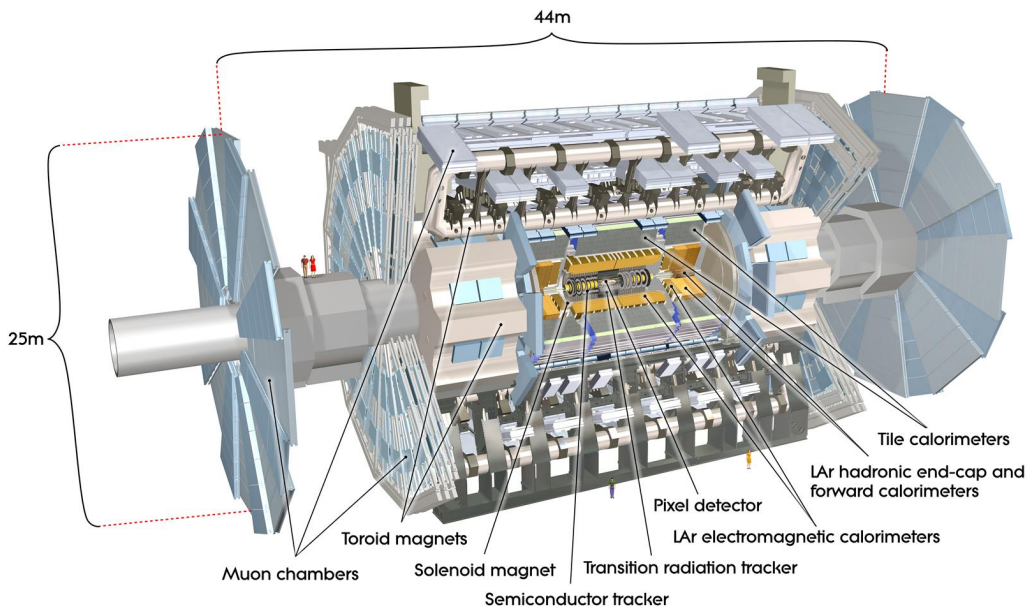


Figure 2.2: The cut-away view of the ATLAS detector. It is 25m high and 44m long. [4]

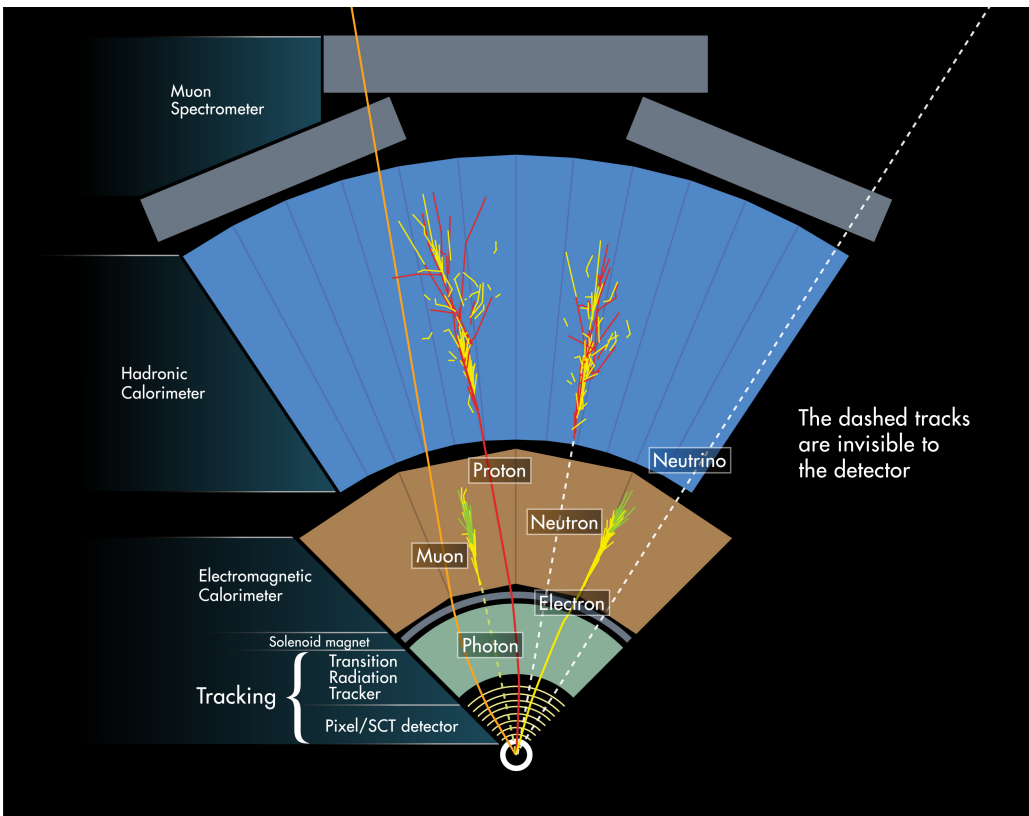


Figure 2.3: The cross section of the ATLAS detector. This shows different components of the ATLAS and how ATLAS detect different types of particles [5]

### 2.3.1 coordinate system

The nominal collision point is defined as the origin of the coordinate system. The z-axis is along the beam direction. The positive x-axis is pointing to the centre of the LHC ring. The positive y-axis is in the upward direction. The azimuthal angle  $\phi$  and the polar angle  $\theta$  are defined as usual in the spherical coordinate system. The pseudorapidity  $\eta$  is defined as:

$$\eta = -\ln \left( \tan \frac{\theta}{2} \right) \quad (2.2)$$

The distance  $\Delta R$  in the pseudorapidity-azimuthal angle space is defined as:

$$\Delta R = \sqrt{(\Delta\phi)^2 + (\Delta\eta)^2} \quad (2.3)$$

The ATLAS detector has a reflection symmetry about the x-y plane.

### 2.3.2 magnetic system

There is a thin superconducting solenoid magnet around the inner detector, which generates a 2 T magnetic field inside the inner detector. There are also 3 large superconducting toroids around the calorimeter: one for barrel and two for end-caps. All these magnets are shown in figure 2.2.

### 2.3.3 The inner detector

The inner detector is a particle tracker. It mainly detects the tracks of charged particles and has good performance for measuring the momentum of the charged particles and locating the position of the vertices. Figure 2.4 shows the whole structure of the inner detector. The inner detector consists of 3 sub-detectors from inner to outer: the pixel detector, the silicon microstrip tracker (SCT) and the transition radiation tracker (TRT). Each part further divides into two parts: the barrel region with smaller  $|\eta|$  and the end-cap region with larger  $|\eta|$ . Figure 2.5 shows the distances  $R$  from the beam for the 3 sub-detectors, and figure 2.6 shows the shapes and the orientations of each sensor and the  $\eta$  coverage, in both the barrel and the end-cap regions. The  $\eta$  coverage for the inner detector is  $|\eta| < 2.5$ . The shapes and the orientations of the sensors are different in the barrel and the end-cap regions. In the barrel region, the shape and the orientation of the sensors is concentric cylinder shells around the beam axis, while in the end-cap region, they are disks perpendicular to the beam axis.

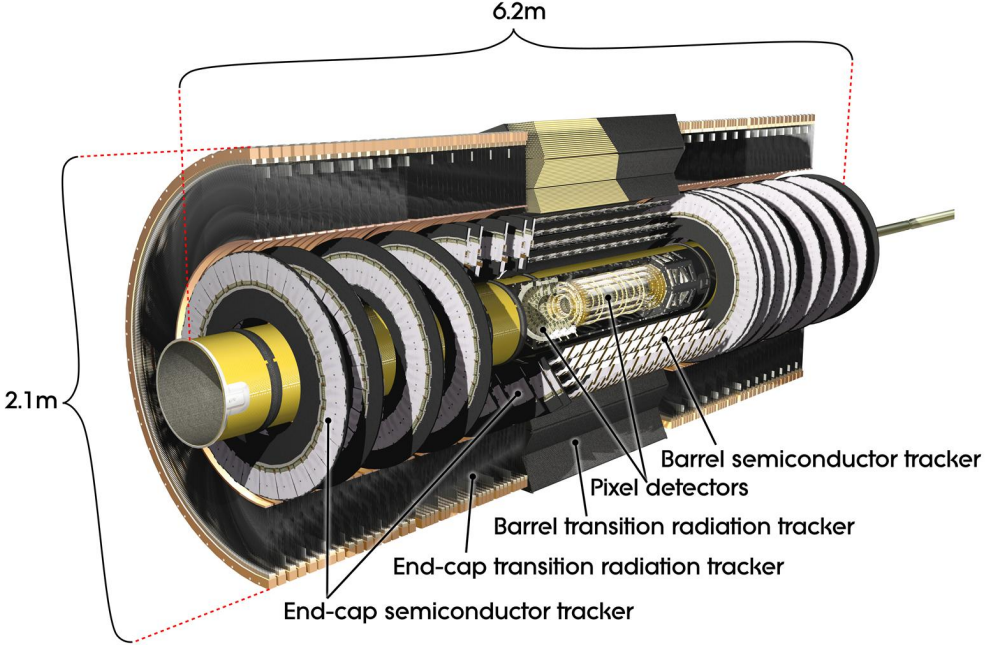


Figure 2.4: The whole structure of the ATLAS inner detector. [6]

The precision tracking detectors (pixels and SCT) has high resolution in space by using discrete space-points to detect the track of a charged particle, with the cutting-edge technology, in order to achieve the good performance of the inner detector. When the particle moves inside the inner detector, there are, in average, 36 hits per one track. By recording the positions of these hits, the path of the particle can be reconstructed. The whole inner detector is immersed in a 2 T magnetic field generated by the solenoid magnet, and hence the path of any charged particles will be bent. By measuring the curvature of the path, the charge and momentum of the particle can be measured. The equation for the circular path is

$$\frac{d\mathbf{p}}{dt} = q(\mathbf{v} \times \mathbf{B}) \quad (2.4)$$

where the relativistic momentum  $\mathbf{p} = \gamma m\mathbf{v}$ .

$$\frac{d\mathbf{p}}{dt} = q\left(\frac{\mathbf{p}}{\gamma m} \times \mathbf{B}\right) \quad (2.5)$$

$$= \frac{q}{\gamma m}(\mathbf{p} \times \mathbf{B}) \quad (2.6)$$

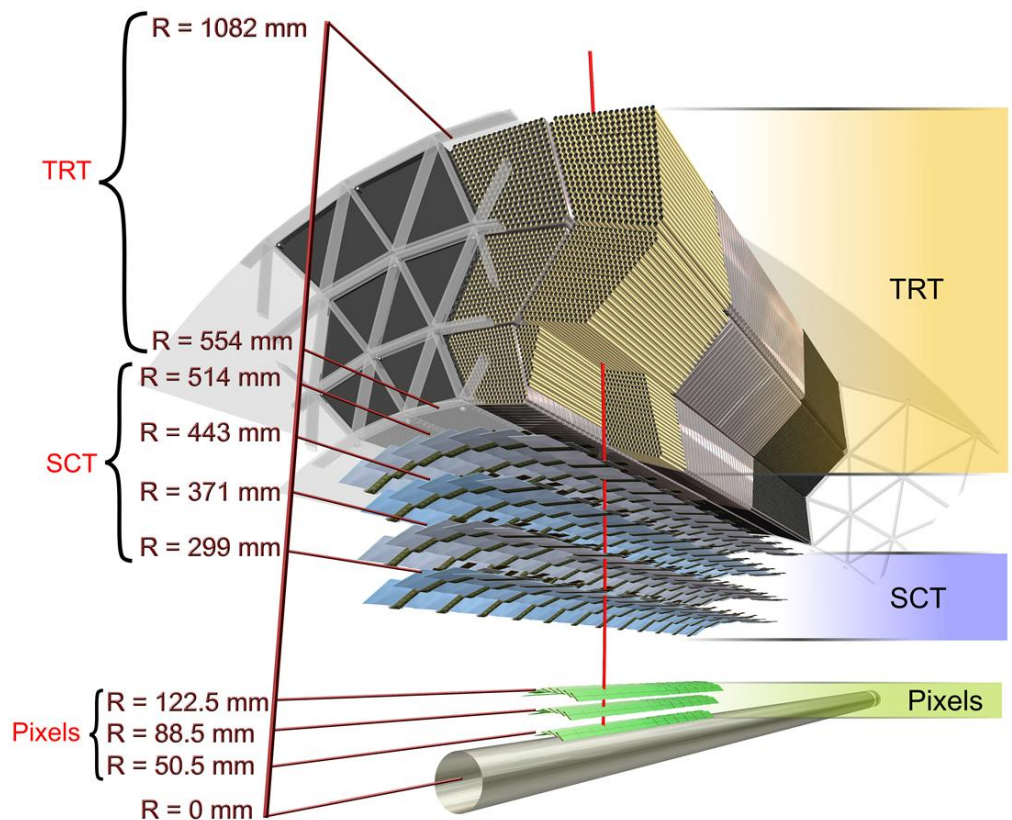


Figure 2.5: The distances  $R$  from the beam for the 3 components: pixel, SCT and TRT. [6]

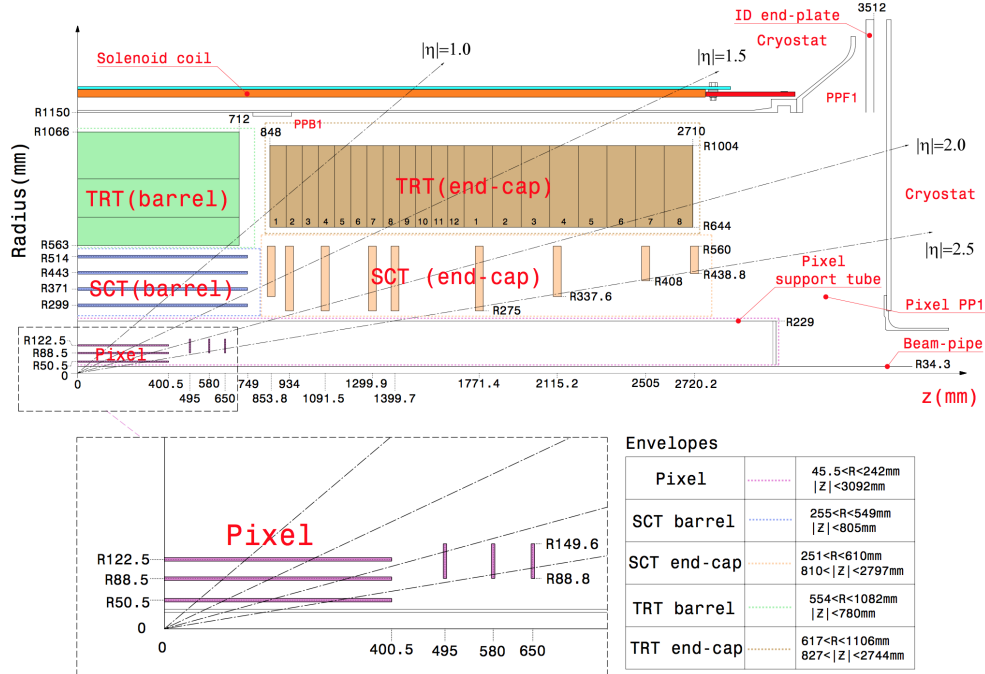


Figure 2.6: The shapes, the orientations and the  $\eta$  coverage for each sensor. [7]

From this equation, we can get the angular frequency  $\omega$ ,

$$\omega = \frac{qB}{\gamma m} \quad (2.7)$$

$$\frac{v}{r} = \frac{qB}{\gamma m} \quad (2.8)$$

$$\frac{1}{r} = \frac{qB}{\gamma mv} \quad (2.9)$$

$$\frac{1}{r} = \frac{qB}{p} \quad (2.10)$$

$$p = rqB \quad (2.11)$$

By this equation, we can calculate the momentum of the particle, from the curvature of track  $1/r$ , the charge and the magnetic field strength.

### 2.3.3.1 Pixel detector

As shown in figure 2.6, there are 3 layers of cylinder in the barrel region, and 3 layers of disk for each end-cap region. There are in total 1744 modules in the pixel detectors. Each module is identical, and has the size of  $19\text{mm} \times 63\text{mm}$ , and  $250\ \mu\text{m}$  thick. The module has 47232 pixels, which has size of  $50\mu\text{m} \times 400\mu\text{m}$ , and hence there are in total 80 million pixels for the whole pixel detector. Each pixel has the accuracy of  $10\mu\text{m} \times 115\mu\text{m}$ . The sensor is using planar n<sup>+</sup>-in-n type of

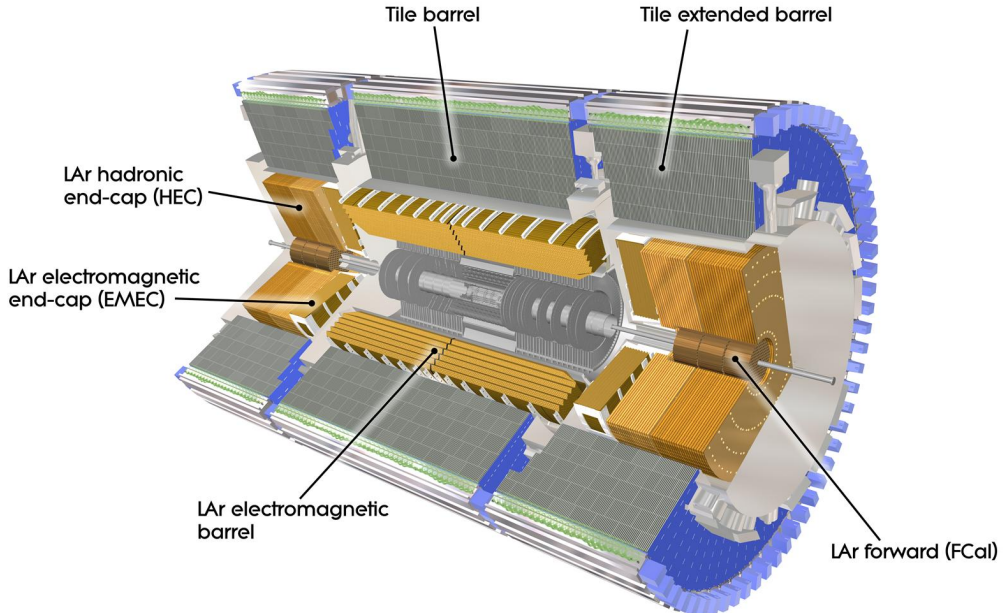


Figure 2.7: whole calorimeter [8]

silicon, with  $n^+$ -type at the readout side and n-type at another side.

### 2.3.3.2 SCT

As shown in figure 2.6, there are 4 layers of cylinder in the barrel region, and 9 layers of disk for each end-cap region. There are in total 4088 modules in the SCT, with the thickness of  $285\ \mu m$ . There are in total 6.3 million pixels for the SCT. Each pixel has the accuracy of  $17\mu m \times 580\mu m$ . The sensor is using planar p-in-n type of silicon.

### 2.3.3.3 TRT

136 TRT modules. TRT in the outer part is to produce and detect the transition radiation from the particle. TRT comprises many layers of gaseous straw tube elements interleaved with transition radiation material. Each pixel has the accuracy of  $130\mu m$ .

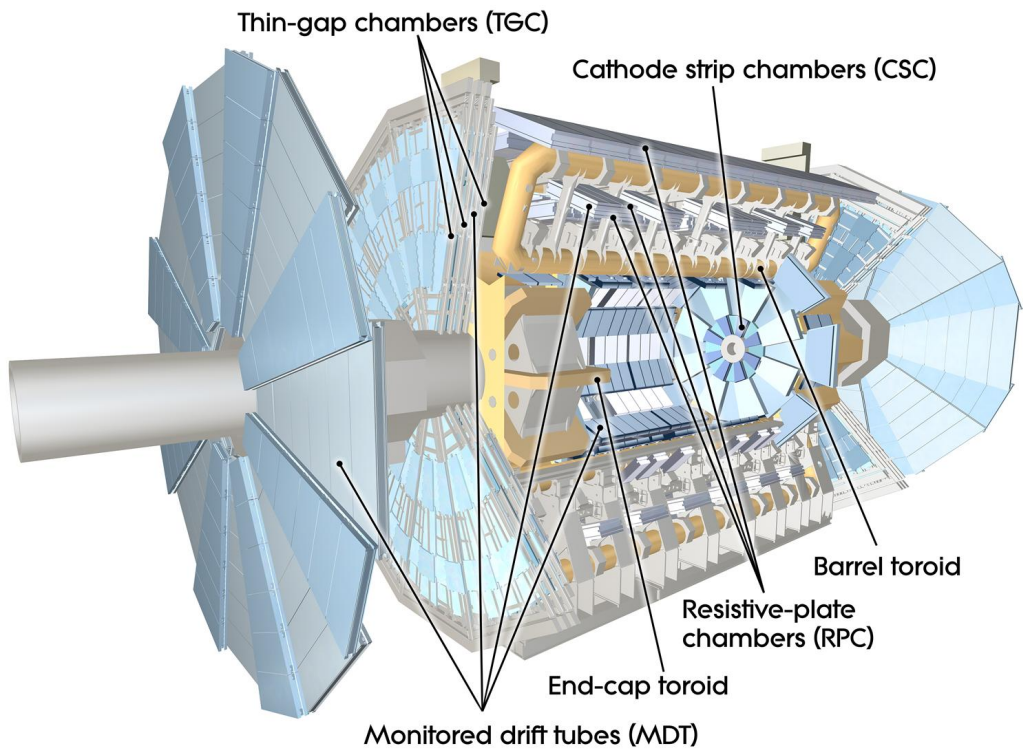


Figure 2.8: muon spectrometer [9]

### 2.3.4 Calorimeter

#### 2.3.4.1 Electromagnetic calorimeter

#### 2.3.4.2 Hardronic calorimeter

### 2.3.5 Muon Spectrometer

# **Chapter 3**

## **Pre-selection**

**3.1 Trigger selection**

**3.2 Event selection**

**3.3 Object definitions**

3.3.1 electrons and muons

3.3.2 jets

3.3.3 Missing transverse energy

## **Chapter 4**

# **Signal Region**

# Chapter 5

## Background estimation

The charge flip background and the fake lepton background are the two dominant backgrounds that their original particles in the final state come from the SM, but not the SUSY signal. Because of the mis-reconstruction, they pass the selections of the SRs. This type of background will be estimated by using the data-driven method.

### 5.1 charge flip background

#### 5.1.1 Sources for charge flip background

The charge flip background is due to the mis-identification of the sign of the charge of a lepton, after the reconstruction. The sign of the charge is determined by the direction of the curvature of the track. There are two main sources for the mis-identification for the direction of the curvature.

The first source is described by the figure 5.1. It is the case that the lepton interacts with the material of the detector, and a photon is emitted by the process of bremsstrahlung. The emitted photon further produces a pair of electron and positron, namely the  $\gamma$  conversion. As shown in figure 5.1, if the most of the energy is carried by the positron  $e^+$  (the purple track), the direction of the curvature of the reconstructed track (the orange track) will be reversed. Thus, the charge of the lepton is flipped. Because the amount of this mis-identification depends on the number of hits with the detector, and hence depends on  $|\eta|$  of the original track.

The second source is described by the figure 5.2. When the  $p_T$  of the lepton

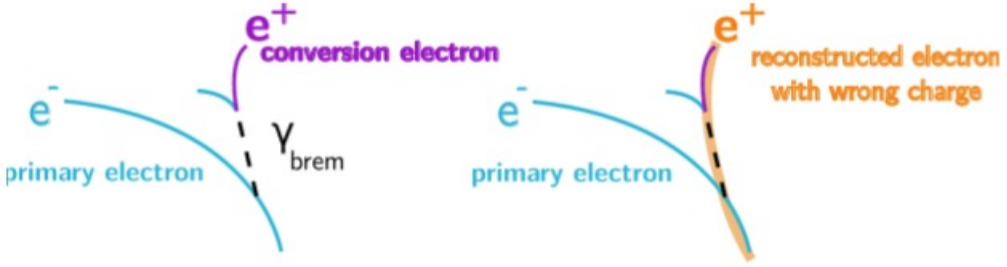


Figure 5.1: This shows how the track of the electron is incorrectly reconstructed (the orange track), due to the process of bremsstrahlung and  $\gamma$  conversion.

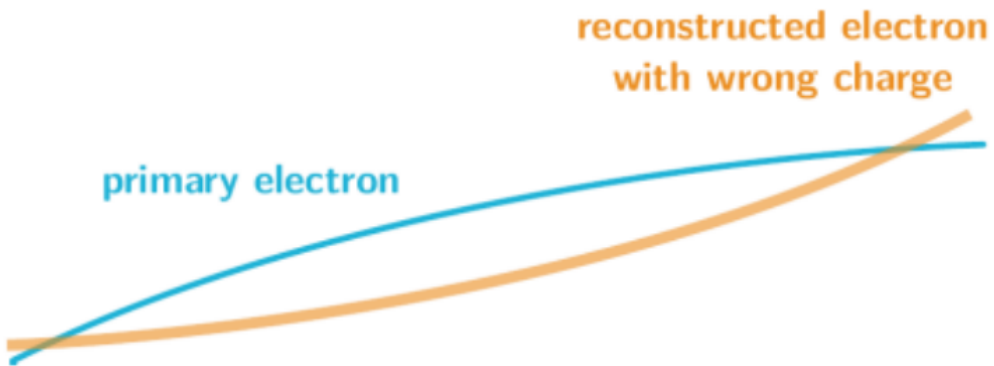


Figure 5.2: This shows how the track of the electron is incorrectly reconstructed (the orange track), due to very high  $p_T$  of the electron.

is very high, the track of the lepton will be almost a straight line. The curvature of the track will be close to zero, and the sign of the curvature will be difficult to distinguish. As a result, the sign of the charge of the lepton will be incorrectly assigned. The chance to have this problem obviously depends on  $p_T$  of the lepton.

Compared to an electron, the charge of a reconstructed muon will be less often to be mis-identified. The first reason is that a muon is heavier than an electron. This will reduce the chance of the process of bremsstrahlung. The second reason is that muons can reach to the muon spectrometer, which is the outer part of the detector, while most electrons cannot. This means that the length of the track of a muon, which can be detected by the tracker, is longer than that of an electron. Hence, the reconstructed curvature of the track for muons can be more accurate, and it reduces the chance of the mis-identification due to the high  $p_T$ . Because most of the charge flip background comes from electrons, we only estimate the

charge flip background for electrons.

### 5.1.2 Likelihood method

The probability that the charge of an electron is mis-identified is denoted by the charge-flip rate  $\epsilon_i$ , where the index  $i$  represents the dependency on the  $p_T$  and  $\eta$  of the electron. The value of index  $i$  is found by splitting the variables  $p_T$  and  $|\eta|$  into different 2-dimensional bins, and the binning for the  $p_T$  and  $|\eta|$  is described by the table 5.1. The index  $i$  of  $\epsilon_i$  is defined by the index of the bin.

Variable	Boundary of the bins
$p_T$ (GeV)	25, 60, 90, 130, 150, 1000
$ \eta $	0, 0.50, 1.00, 1.37, 1.52, 1.80, 2.00, 2.47

Table 5.1: Binning in  $p_T$  and  $|\eta|$  for the charge-flip rate  $\epsilon_i$ .

Suppose that, before the reconstruction, there are  $m_{OS}^{ij}$  opposite-sign events with the leading lepton in bin  $i$  and the subleading lepton in bin  $j$ , and similarly there are  $m_{SS}^{ij}$  same-sign events. After the reconstruction, due to the charge flip, there are  $M_{OS}^{ij}$  opposite-sign events and  $M_{SS}^{ij}$  same-sign events. The number of events after the reconstruction is given by

$$M_{OS}^{ij} = (1 - \epsilon_i)(1 - \epsilon_j)m_{OS}^{ij} + \epsilon_i(1 - \epsilon_j)m_{SS}^{ij} + (1 - \epsilon_i)\epsilon_j m_{SS}^{ij} + \epsilon_i\epsilon_j m_{OS}^{ij} \quad (5.1)$$

$$M_{SS}^{ij} = (1 - \epsilon_i)(1 - \epsilon_j)m_{SS}^{ij} + \epsilon_i(1 - \epsilon_j)m_{OS}^{ij} + (1 - \epsilon_i)\epsilon_j m_{OS}^{ij} + \epsilon_i\epsilon_j m_{SS}^{ij} \quad (5.2)$$

From equation 5.2, the number of reconstructed same-sign events due to the real opposite-sign events, i.e. the charge flip BG , denoted by  $N_{SS}^{ij}$ , is

$$N_{SS}^{ij} = \epsilon_i(1 - \epsilon_j)m_{OS}^{ij} + (1 - \epsilon_i)\epsilon_j m_{OS}^{ij} \quad (5.3)$$

In the SRs,  $m_{OS}^{ij}$  is the number of OS events before the reconstruction, but finally pass all selections in SRs.  $M_{OS}^{ij}$  is the total number of events that pass all selections in SRs, but replace SS requirement by OS. Because  $m_{OS}^{ij}$  is much larger than  $m_{SS}^{ij}$  and the measured charge-flip rate  $\epsilon_i$  is about  $10^{-3}$ ,  $m_{OS}^{ij}$  can be estimated by

$$M_{OS}^{ij} \approx (1 - \epsilon_i)(1 - \epsilon_j)m_{OS}^{ij} \quad (5.4)$$

$$m_{OS}^{ij} \approx \frac{M_{OS}^{ij}}{(1 - \epsilon_i)(1 - \epsilon_j)} \quad (5.5)$$

$$m_{OS}^{ij} \approx M_{OS}^{ij} \quad (5.6)$$

$$m_{OS}^{ij} \approx M_{OS}^{ij} + M_{SS}^{ij} \quad (5.7)$$

By substituting equation 5.7 into 5.3, the charge flip BG can be estimated by  $M_{OS}^{ij}$ ,  $M_{SS}^{ij}$  and the charge-flip rate  $\epsilon_i$ ,

$$N_{SS}^{ij} = \epsilon_i(1 - \epsilon_j)m_{OS}^{ij} + (1 - \epsilon_i)\epsilon_jm_{OS}^{ij} \quad (5.8)$$

$$= [\epsilon_i(1 - \epsilon_j) + (1 - \epsilon_i)\epsilon_j]m_{OS}^{ij} \quad (5.9)$$

$$\approx p_{ij}(M_{OS}^{ij} + M_{SS}^{ij}) \quad (5.10)$$

$$= p_{ij}N^{ij} \quad (5.11)$$

where  $p_{ij}$  and  $N^{ij}$  are

$$\begin{aligned} p_{ij} &= \epsilon_i(1 - \epsilon_j) + (1 - \epsilon_i)\epsilon_j \\ N^{ij} &= M_{OS}^{ij} + M_{SS}^{ij} \end{aligned} \quad (5.12)$$

The probability density function of  $N_{SS}^{ij}$ , with the given values of  $N^{ij}$  and  $\epsilon_i$ , can be described by the Poisson distribution with the mean value  $\lambda = p_{ij}N^{ij}$ .

$$P(N_{SS}^{ij}|N^{ij}, \epsilon_i, \epsilon_j) = \frac{\lambda^{N_{SS}^{ij}}e^{-\lambda}}{N_{SS}^{ij}!} \quad (5.13)$$

$$= \frac{(p_{ij}N^{ij})^{N_{SS}^{ij}}e^{-p_{ij}N^{ij}}}{N_{SS}^{ij}!} \quad (5.14)$$

In order to estimate the charge flip BG, we need to measure the charge-flip rate  $\epsilon_i$ . The charge-flip rate is measured as a function of  $p_T$  and  $|\eta|$  by using a likelihood method, based on the 2015 and 2016 data. A control region is used to select  $Z \rightarrow ee$  processes. Inside the control region, exactly 2 signal electrons are required. Also, a Z mass window of  $80 \text{ GeV} < m_{ll} < 100 \text{ GeV}$  is used. In this control region, the total number of events  $N^{ij}$  and the SS events  $N_{SS}^{ij}$  in each bin can be measured. By using the equation 5.14, the charge-flip rate  $\epsilon_i$  can be measured by using the following likelihood method.

The likelihood function  $L$  is defined by

$$L(\epsilon_i, \epsilon_j|N^{ij}, N_{SS}^{ij}) = \prod_{ij} P(N_{SS}^{ij}|N^{ij}, \epsilon_i, \epsilon_j) \quad (5.15)$$

$$= \prod_{ij} \frac{(p_{ij}N^{ij})^{N_{SS}^{ij}}e^{-p_{ij}N^{ij}}}{N_{SS}^{ij}!} \quad (5.16)$$

$$(5.17)$$

Given the measured values of  $N^{ij}$  and  $N_{SS}^{ij}$  in each bin, by maximizing the likelihood function over all possible values of  $\epsilon_i$ , the value of  $\epsilon_i$  can be estimated. By

taking the negative logarithm, it is equivalent to minimize  $-\ln L$ .

$$-\ln L = -\ln \prod_{ij} \frac{(p_{ij} N_{SS}^{ij})^{N_{SS}^{ij}} e^{-p_{ij} N_{SS}^{ij}}}{N_{SS}^{ij}!} \quad (5.18)$$

$$= -\sum_{ij} \ln \frac{(p_{ij} N_{SS}^{ij})^{N_{SS}^{ij}} e^{-p_{ij} N_{SS}^{ij}}}{N_{SS}^{ij}!} \quad (5.19)$$

$$= -\sum_{ij} \left[ N_{SS}^{ij} \ln(p_{ij} N_{SS}^{ij}) - p_{ij} N_{SS}^{ij} - \ln(N_{SS}^{ij}!) \right] \quad (5.20)$$

$$= -\sum_{ij} \left[ N_{SS}^{ij} \ln(p_{ij} N_{SS}^{ij}) - p_{ij} N_{SS}^{ij} \right] + \text{constant} \quad (5.21)$$

$$= -\sum_{ij} \left[ N_{SS}^{ij} \ln(N^{ij}[\epsilon_i(1-\epsilon_j) + (1-\epsilon_i)\epsilon_j]) - N^{ij}[\epsilon_i(1-\epsilon_j) + (1-\epsilon_i)\epsilon_j] \right] + \text{constant} \quad (5.22)$$

### 5.1.3 Background subtraction

By minimizing  $-\ln L$  described in the previous section, the value of the charge-flip rate  $\epsilon_i$  can be measured by using the data in the control region. In order to have better input values of  $N^{ij}$  and  $N_{SS}^{ij}$ , the number of events should mainly come from  $Z \rightarrow ee$  processes, and other processes should be subtracted. The number of events from other processes can be estimated by the sideband region:  $60 \text{ GeV} < m_{ll} < 80 \text{ GeV}$  and  $100 \text{ GeV} < m_{ll} < 120 \text{ GeV}$ . The corrected values of  $N^{ij}$  and  $N_{SS}^{ij}$  are given by

$$N_{80,100;\text{corrected}} = N_{80,100} - 20 \left( \frac{N_{60,80} + N_{80,100}}{20 + 20} \right) \quad (5.23)$$

In the sideband subtraction, the number of events in the sideband region should be normalized to the width of the central region. In general, given the number of events in the central region  $N_{\text{central}}$ , the left sideband region  $N_{\text{left}}$  and the right sideband region  $N_{\text{right}}$ , and their corresponding width  $w_{\text{central}}$ ,  $w_{\text{left}}$  and  $w_{\text{right}}$ , the corrected values  $N_{\text{central},\text{corrected}}$  are given by

$$N_{\text{central},\text{corrected}} = N_{\text{central}} - w_{\text{central}} \left( \frac{N_{\text{left}} + N_{\text{right}}}{w_{\text{left}} + w_{\text{right}}} \right) \quad (5.24)$$

### 5.1.4 Results without systematic uncertainty

Figure 5.3 shows the measured values of the charge-flip rate  $\epsilon_i$  by using the data. The errors only include the uncertainties in the likelihood method due to the statistics, denoted by  $\epsilon_{\text{lik,data}}$ .

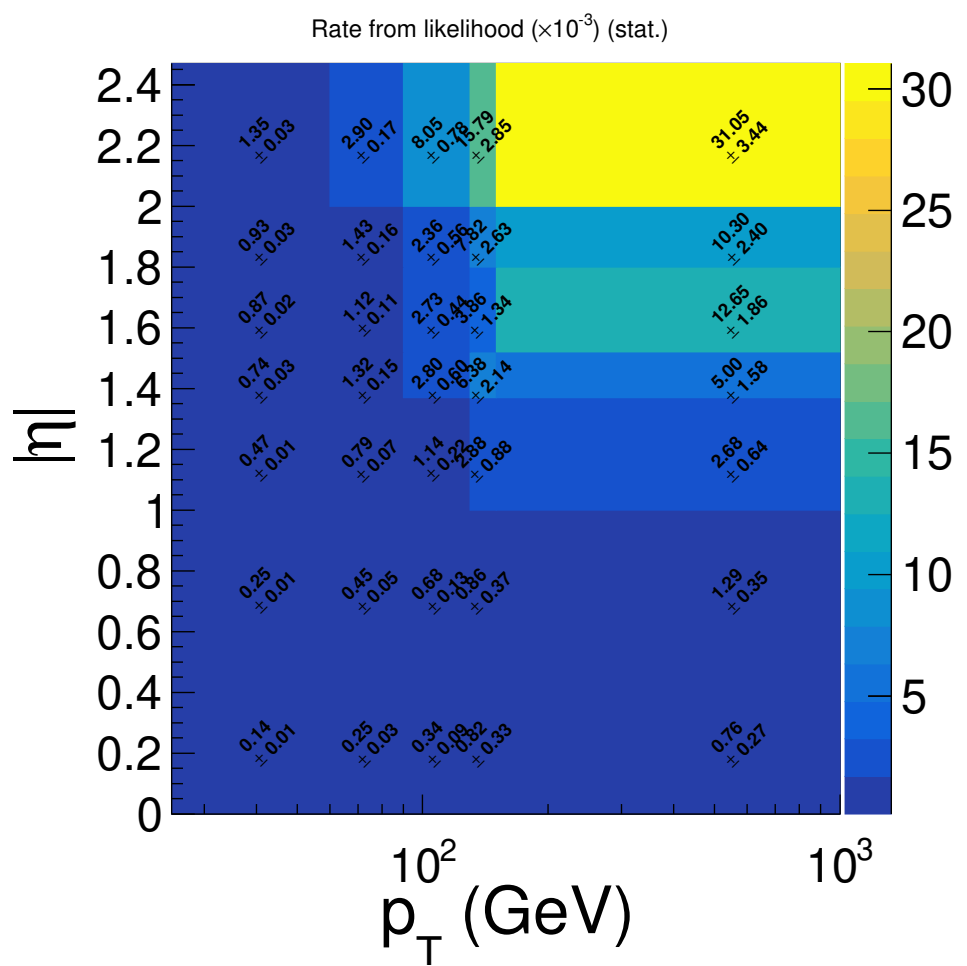


Figure 5.3: The measured values of the charge-flip rate  $\epsilon_i$  in data. Only uncertainties due to the likelihood method are included.

### 5.1.5 Systematic uncertainties due to background subtraction

The systematic uncertainties due to background subtraction is estimated by the variations of different central widths and sideband widths. The following are the nominal central region and sideband region, and their 4 variations.

The nominal background subtraction:

- Central region: 80 - 100 GeV; Sideband width: 20 GeV

The 4 variations for background subtraction:

- Central region: 80 - 100 GeV; Sideband width: 15 GeV
- Central region: 80 - 100 GeV; Sideband width: 25 GeV
- Central region: 75 - 105 GeV; Sideband width: 20 GeV
- Central region: 80 - 100 GeV; no background subtraction

For each bin, the largest deviation from the nominal among these variations is the systematic uncertainty due to background subtraction.

$$\sigma_{\text{bgk}} = \max\{|\sigma_{\text{nominal}} - \sigma_{\text{variation}}|\} \quad (5.25)$$

Figure 5.4 shows the variations of the resulting charge flip rate, due to these 4 variations.

### 5.1.6 Systematic uncertainties due to likelihood method

The systematic uncertainties due to likelihood method are estimated by the difference between the likelihood method and the MC truth method. In the MC truth method, the charge-flip rate is estimated by using the truth information in  $Z \rightarrow ee$  MC samples inside the control region. The control region requires exactly 2 signal electrons. The following are the procedures to match the reconstructed electron to the original electron, and hence the original electric charge can be found. Figure 5.5 shows how the original electron is found in the decay process described in figure 5.1. In this procedure, some reconstructed electrons will be ignored.

1. The reconstructed electron will be matched to the truth particle with the smallest  $\Delta R$  within the cone  $\Delta R < 0.1$ . If no any truth particles can be found inside the cone, the reconstructed electron will be ignored.

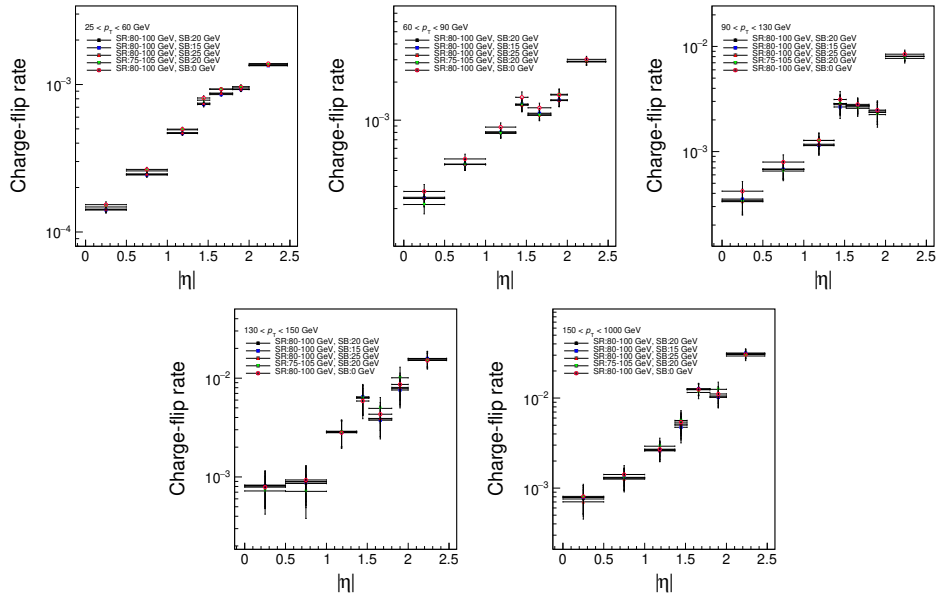


Figure 5.4: The systematic variations of the charge-flip rate  $\epsilon_i$  in data, due to the background subtraction.

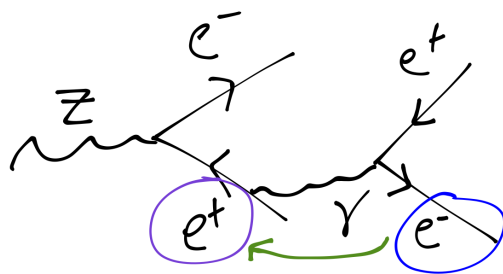


Figure 5.5: This diagram shows how the original electron is found through the decay chain.

2. If the truth particle is not an electron, it will be ignored.
3. If the origin of the truth electron is not a Z boson, it will be ignored.
4. If the daughter particle of the Z boson is not an electron, it will be ignored.
5. The charge of the daughter electron from the Z boson is the original charge of the reconstructed electron.

Only the events with two reconstructed electrons that are not ignored in the above procedure are considered.  $N_{\text{total}}$  is the total number of electrons in these events, and  $N_{\text{flipped}}$  is the number of electrons that the original charge and the reconstructed charge are different. By calculating the ratio in each bin, the charge flip rate can be estimated by using the MC truth information.

$$\epsilon_{\text{MC truth}} = \frac{N_{\text{flipped}}}{N_{\text{total}}} \quad (5.26)$$

The systematic uncertainties due to likelihood method  $\sigma_{\text{truth}}$  is then given by for MC,

$$\sigma_{\text{truth,MC}} = |\epsilon_{\text{lik,MC}} - \epsilon_{\text{MC truth}}| \quad (5.27)$$

for data,

$$\sigma_{\text{truth,data}} = \epsilon_{\text{lik,data}} \times \frac{\sigma_{\text{truth,MC}}}{\epsilon_{\text{lik,MC}}} \quad (5.28)$$

Figure 5.6 shows the comparison of the resulting charge flip rate, between the likelihood method and the MC truth method, by using the  $Z \rightarrow ee$  MC samples.

### 5.1.7 Results with total uncertainties

The total systematic uncertainties is the quadratic sum of systematic uncertainties due to the background subtraction and the likelihood method, described in section 5.1.5 and 5.1.6 respectively.

$$\sigma_{\text{sys}} = \sqrt{\sigma_{\text{bgk}}^2 + \sigma_{\text{truth}}^2} \quad (5.29)$$

The total uncertainties is the quadratic sum of the total systematic uncertainties and the statistical uncertainties in the likelihood method.

$$\sigma_{\text{tot}} = \sqrt{\sigma_{\text{sys}}^2 + \sigma_{\text{lik}}^2} \quad (5.30)$$

Figure 5.7 shows the measured values of the charge-flip rate  $\epsilon_i$  by using the data, with total uncertainties described in equation 5.30.

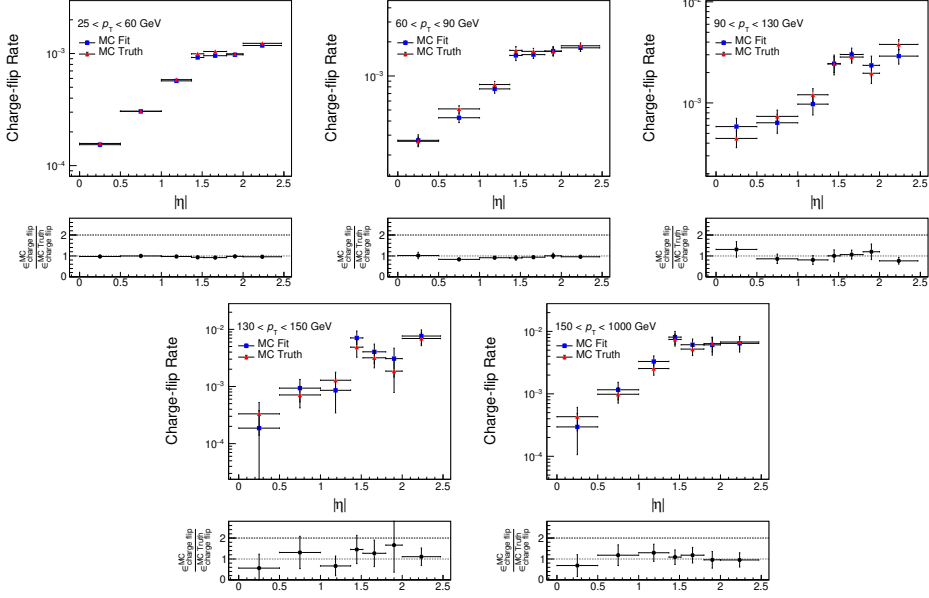


Figure 5.6: The comparison between the likelihood method and the MC truth method, by using the  $Z \rightarrow ee$  MC samples. Hence, the systematic uncertainties due to likelihood method can be estimated.

### 5.1.8 MC validation

The charge flip rate can be validated by using the  $Z \rightarrow ee$  MC samples. By using the equation 5.5 and 5.9,  $N_{SS}^{ij}$  can be approximated by

$$N_{SS}^{ij} = [\epsilon_i(1 - \epsilon_j) + (1 - \epsilon_i)\epsilon_j]m_{OS}^{ij} \quad (5.31)$$

$$\approx [\epsilon_i(1 - \epsilon_j) + (1 - \epsilon_i)\epsilon_j] \frac{M_{OS}^{ij}}{(1 - \epsilon_i)(1 - \epsilon_j)} \quad (5.32)$$

$$= \frac{\epsilon_i(1 - \epsilon_j) + (1 - \epsilon_i)\epsilon_j}{(1 - \epsilon_i)(1 - \epsilon_j)} M_{OS}^{ij} \quad (5.33)$$

Also, in the equation 5.2,  $m_{SS}^{ij}$  is zero for the  $Z \rightarrow ee$  MC samples, we have

$$M_{SS}^{ij} = \epsilon_i(1 - \epsilon_j)m_{OS}^{ij} + (1 - \epsilon_i)\epsilon_j m_{OS}^{ij} \quad (5.34)$$

$$= N_{SS}^{ij} \quad (5.35)$$

Hence, it is expected that

$$M_{SS}^{ij} \approx \frac{\epsilon_i(1 - \epsilon_j) + (1 - \epsilon_i)\epsilon_j}{(1 - \epsilon_i)(1 - \epsilon_j)} M_{OS}^{ij} \quad (5.36)$$

By weighting the OS events in MC with the weight,

$$\text{weight} = \frac{\epsilon_i(1 - \epsilon_j) + (1 - \epsilon_i)\epsilon_j}{(1 - \epsilon_i)(1 - \epsilon_j)} \quad (5.37)$$

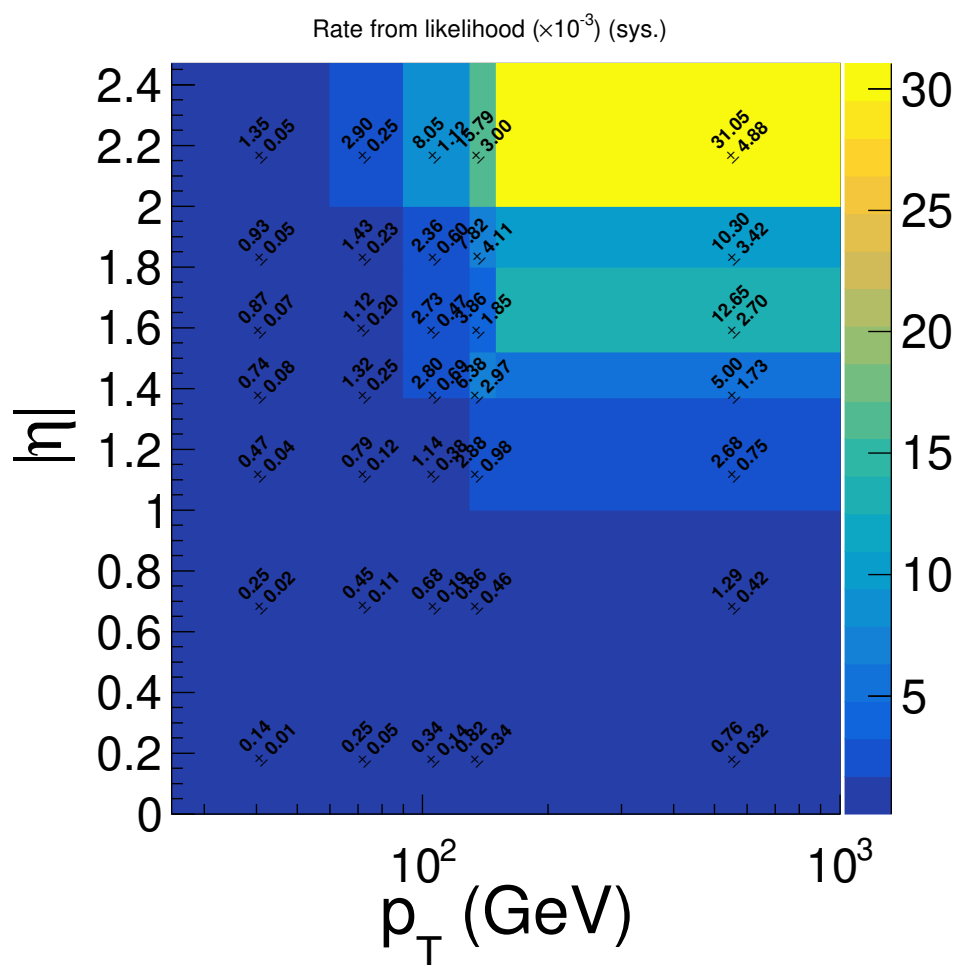


Figure 5.7: The measured values of the charge-flip rate  $\epsilon_i$  in data, with total uncertainties.

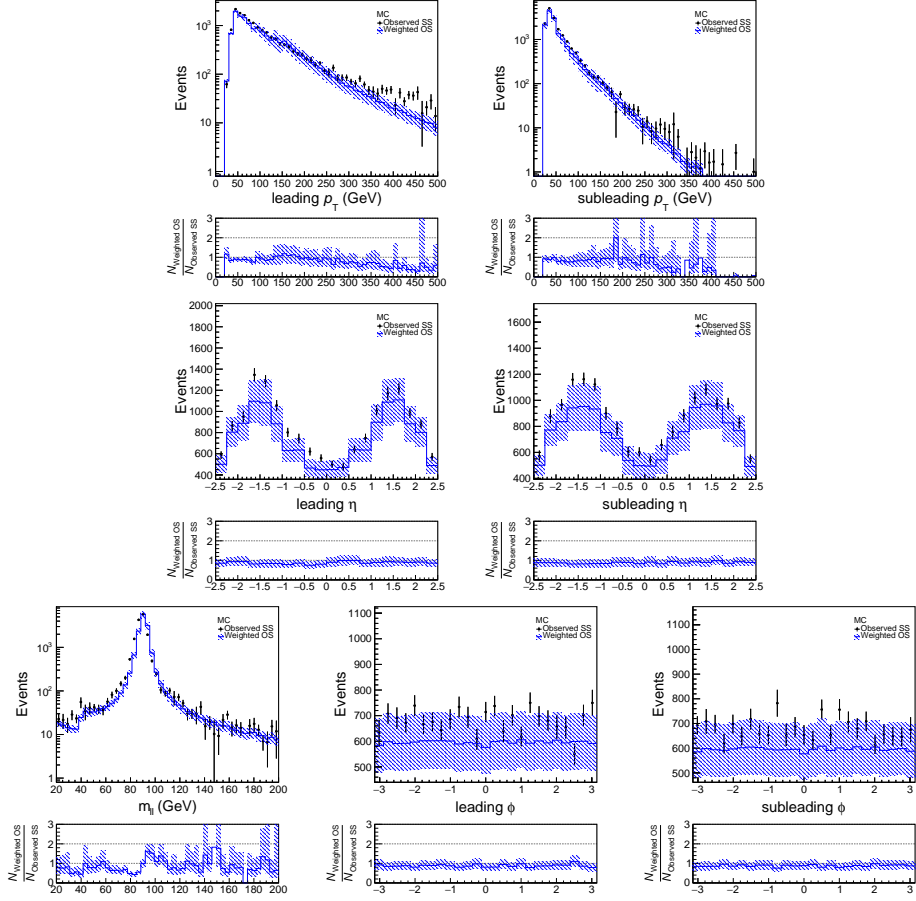


Figure 5.8: The comparison between the weighted OS events and the SS events, with different variables.

the weighted OS events and the SS events will be close to each other. This can be used to validate the charge flip rate. Figure shows the comparison between the weighted OS events and the SS events, with different variables. All event weights are applied, except the charge flip scale factor. The weighted OS events and the SS events agree within the uncertainties.

## 5.2 fake lepton background

## Chapter 6

# Validation regions

# References

- [1] *Standard Model of Elementary Particles*,  
[https://en.wikipedia.org/wiki/File:Standard\\_Model\\_of\\_Elementary\\_Particles.svg](https://en.wikipedia.org/wiki/File:Standard_Model_of_Elementary_Particles.svg).
- [2] *Standard Model Feynman Diagram Vertices*,  
[https://en.wikipedia.org/wiki/File:Standard\\_Model\\_Feynman\\_Diagram\\_Vertices.png](https://en.wikipedia.org/wiki/File:Standard_Model_Feynman_Diagram_Vertices.png).
- [3] E. Mobs, *The CERN accelerator complex. Complexe des accélérateurs du CERN*, <https://cds.cern.ch/record/2197559>, General Photo.
- [4] J. Pequenao, *Computer generated image of the whole ATLAS detector*,  
<https://cds.cern.ch/record/1095924>.
- [5] J. Pequenao and P. Schaffner, *An computer generated image representing how ATLAS detects particles*, <https://cds.cern.ch/record/1505342>.
- [6] J. Pequenao, *Computer generated image of the ATLAS inner detector*,  
<https://cds.cern.ch/record/1095926>.
- [7] G. Aad, E. Abat, and J. Abdallah, *The ATLAS Experiment at the CERN Large Hadron Collider*, Journal of Instrumentation **3** (2008) S08003,  
<http://stacks.iop.org/1748-0221/3/i=08/a=S08003>.
- [8] J. Pequenao, *Computer Generated image of the ATLAS calorimeter*,  
<https://cds.cern.ch/record/1095927>.
- [9] J. Pequenao, *Computer generated image of the ATLAS Muons subsystem*,  
<https://cds.cern.ch/record/1095929>.
- [10] *The accelerator complex*, <https://home.cern/about/accelerators>.

- [11] *Pulling together: Superconducting electromagnets*,  
[https://home.cern/about/engineering/  
pulling-together-superconducting-electromagnets.](https://home.cern/about/engineering/pulling-together-superconducting-electromagnets)
- [12] *Cryogenics: Low temperatures, high performance*, [https://home.cern/  
about/engineering/cryogenics-low-temperatures-high-performance.](https://home.cern/about/engineering/cryogenics-low-temperatures-high-performance)